NANO LETTERS

Letter

pubs.acs.org/NanoLett

Electrochemical Reaction in Single Layer MoS_2: Nanopores Opened Atom by Atom

J. Feng,[†] K. Liu,*[,†] M. Graf,[†] M. Lihter,[†,‡] R. D. Bulushev,[†] D. Dumcenco,[§] D. T. L. Alexander,[∥] D. Krasnozhon,[§] T. Vuletic,[‡] A. Kis,[§] and A. Radenovic*[,†]

[†]Laboratory of Nanoscale Biology, Institute of Bioengineering, School of Engineering, EPFL, 1015 Lausanne, Switzerland

[‡]Institut za fiziku, Bijenička 46, Zagreb, Croatia

[§]Laboratory of Nanoscale Electronics and Structure, Institute of Electrical Engineering, School of Engineering, EPFL, 1015 Lausanne, Switzerland

[∥]Centre Interdisciplinaire de Microscopie Électronique (CIME), EPFL, 1015 Lausanne, Switzerland

S *Supporting Information*

ABSTRACT: Ultrathin nanopore membranes based on 2D materials have demonstrated ultimate resolution toward DNA sequencing. Among them, molybdenum disulfide (MoS_2) shows long-term stability as well as superior sensitivity enabling high throughput performance. The traditional method of fabricating nanopores with nanometer precision is based on the use of focused electron beams in transmission electron microscope (TEM). This nanopore fabrication process is time-consuming, expensive, not scalable, and hard to control below 1 nm. Here, we exploited the electrochemical activity of MoS_2 and developed a convenient and scalable method to controllably make nanopores in single-layer MoS_2 with subnanometer precision using electrochemical reaction (ECR). The electrochemical reaction on the surface of single-layer MoS_2 is initiated at the location of defects or single atom vacancy, followed by the successive removals of individual atoms or unit cells from single-layer MoS_2 lattice and finally formation of a nanopore. Step-like features in the ionic current through the growing nanopore provide direct feedback on the nanopore size inferred from a widely used conductance vs pore size model. Furthermore, DNA translocations can be detected in situ when as-fabricated MoS_2 nanopores are used. The atomic resolution and accessibility of this approach paves the way for mass production of nanopores in 2D membranes for potential solid-state nanopore sequencing.

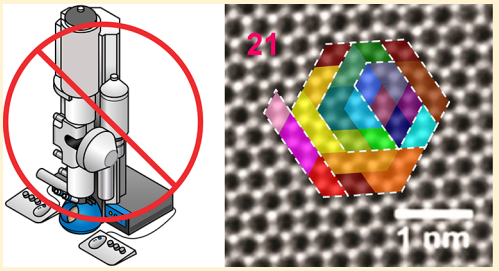

KEYWORDS: *Solid-state nanopores, 2D materials, molybdenum disulfide (MoS_2), electrochemical reaction (ECR), DNA translocation*

Fabrication of nanostructures with subnanometer or even single-atom precision has been a long-term goal for nanotechnology. The rise of graphene[1] and recently other 2D materials, such as the single-layer molybdenum disulfide (MoS_2),[2] offers an ideal platform for such a purpose, due to their highly ordered lattice in two dimensions. Fabrication of solid-state nanopores that are used in single-molecule sensing[3,4] would benefit tremendously from such a nanoscale fabrication method. Conceptually, nanopore sensing is based on a single, nanometer sized aperture located on a nanometer thin membrane; by monitoring the changes in the ionic current it is possible to detect electrophoretically driven biomolecular translocations in a high throughput manner, while revealing localized information on the analyte. Although conceptually simple, the method is still limited to laboratory use[5] since the formation of a single solid-state nanopore with subnanometer precision relies heavily on high-end instrumentation, such as a transmission electron microscope (TEM)[5] and a well-trained TEM user. This nanopore fabrication process is time-consuming, expensive, not scalable, and hard to control below 1 nm. Many efforts, such as chemical wet-etching of silicon[6] or polyethylene terephthalate film[7] have been carried out toward mass production of nanopores. Recently, a pioneering and simple method has been reported using controlled dielectric breakdown to make individual nanopores (3−30 nm diameter) on insulating silicon nitride membranes (5−30 nm thick) without the need of TEM.[8,9]

Among solid-state pores, the highest signal to noise ratio (SNR) and sensitivity has been reported for the atomically thin nanopore membranes made from 2D materials, such as graphene,[10−12] boron nitride,[13] and MoS_2.[14] Theoretically, base by base recognition can be achieved since membrane thicknesses have comparable values with the base-stacking distance (0.34 nm). Therefore, they hold promise for the so-called third generation DNA sequencers. Recently, we have demonstrated the first realization of single nucleotide identification in small MoS_2 nanopores (<4 nm), where we introduced a viscosity gradient system based on room temperature ionic liquids (RTILs) to slow down DNA translocation.[15] The differentiation of nucleotides is based on

Received: February 25, 2015
Revised: April 4, 2015

ACS Publications © XXXX American Chemical Society

DOI: 10.1021/acs.nanolett.5b00768
Nano Lett. XXXX, XXX, XXX−XXX

their ionic current signal and relies strongly on the pore diameter.[15] A controllable nanopore fabrication method, which allows mass production of MoS_2 nanopores below 4 nm with atomic precision, is therefore highly desired.

MoS_2, as a member of transition metal dichalcogenide (TMD) family, has rich electrochemical properties such as catalytic hydrogen generation.[16] During the past several decades, scanning probe microscopes (SPMs) such as scanning tunneling microscopes (STM) and atomic force microscopes (AFM), demonstrated the ability to craft nanostructures with an atom/molecule resolution. In SPM, using tip-induced electrochemical reaction, it is possible to engineer nanostructures or make holes in layered TMDs (WSe_2, $SnSe_2$, $MoSe_2$, or MoS_2). The mechanism can be understood as a surface electrochemical reaction scheme induced via the electric field generated by the SPM tip.[17,18] The oxidation process starts preferably at the surface defects when the voltage threshold (1.2 V in the case of WSe_2)[19] for oxidation is reached and allows variety of nanoengineering means. However, it is still challenging to make nanopores on suspended membranes using SPMs, while implementation of SPMs instrument in nanopore fabrication is comparable to TEMs in terms of cost and complexity.

Here we present in situ application of the electrochemical reaction (ECR) for fabrication of individual nanopores on single-layer MoS_2, with the electric field generated by Ag/AgCl electrodes away from the membrane. ECR starts for a certain critical voltage bias at a defect/vacancy present in the MoS_2 membrane.

Importantly, in the course of ECR fabrication we observe, and we are able to control, the successive removal of single or few MoS_2 units from the monolayer MoS_2 membranes. In this way we accomplish the atom-by-atom nanopore engineering. To the best of our knowledge, this is the first example of nanopore engineering on single-layer MoS_2 membranes with atomic precision utilizing ECR.

The procedure for fabricating MoS_2 nanopores using ECR is schematically illustrated in Figure 1a, where two chambers (cis and trans) are filled with aqueous buffer (1 M KCl, pH 7.4) and biased by a pair of Ag/AgCl electrodes, which are separated by a single-layer MoS_2 membrane. Presence of an active site such as single-atom vacancy[19] facilitates the removal of individual atoms and MoS_2 unit cells from MoS_2 lattice by ECR at voltages higher than the oxidation potential of MoS_2 in aqueous media. This process is facilitated by the electric field focusing by the pore itself. To form freestanding membranes, CVD-grown monolayer MoS_2[20] transferred from a sapphire substrate is suspended over focused ion beam (FIB) defined openings that ranged from 80 to 300 nm in diameter and were centered in a 20 nm thick SiN_x membrane (see Figure 1b). A typical optical image of the transferred triangular flake of CVD-grown monolayer MoS_2 on the supporting silicon nitride membrane is shown in Figure 1c. The freestanding MoS_2 membrane above the FIB defined opening can be further identified under TEM with low magnification (5k×) as shown in Figure 1d. MoS_2 flake is further characterized by energy-dispersive X-ray spectroscopy (EDX) in TEM to reveal the chemical composition. Elements of Mo and S are abundant in the triangular areas as shown in Figure S1. When moving to the high magnification (1M×) and focusing on the freestanding portion of MoS_2 over the FIB opening, the atomic structure of MoS_2 can be clearly resolved as shown in Figure 1e, and the

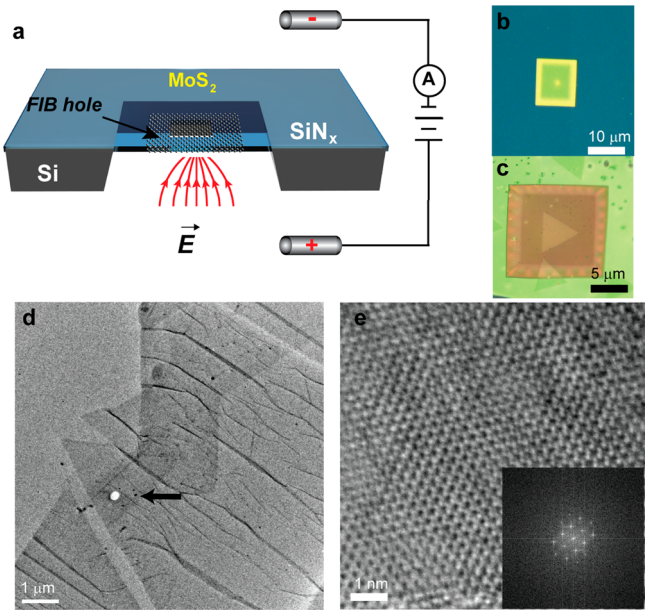

Figure 1. (a) Schematic illustration of preparation of a freestanding MoS_2 membrane ready for electrochemical formation of a nanopore. In the center of the supporting 20 nm thick SiN_x membrane a single focused ion beam, FIB hole is drilled to suspend a small portion of an intact monolayer MoS_2 flake. A single chip is mounted in the flow-cell for typical translocation experiments. A pair of Ag/AgCl electrodes connected to a preamplifier is used to apply transmembrane voltage. (b) An optical image of the SiN_x membrane with a FIB drilled hole in the center. (c) An optical image of the SiN_x membrane with transferred triangular CVD-grown MoS_2 monolayer. (d) Low magnification TEM image of transferred CVD-grown MoS_2 monolayer covering the FIB hole. The FIB hole is indicated by the black arrow. (e) Conventional high-resolution TEM image of the lattice of MoS_2 suspended over the FIB hole. The corresponding diffractogram is shown in the inset.

diffractogram reflects the hexagonal symmetry of MoS_2, as shown in the inset of Figure 1e.

When an intact MoS_2 membrane is mounted into a custom-made microfluidic flow-cell filled with an aqueous buffer, transmembrane potential is applied using a pair of Ag/AgCl electrodes. For a voltage bias below the potential for electrochemical oxidation, small leakage current is normally detected, typically on the order from tens to hundreds of picoamperes depending on the number of defects in the 2D membrane.[21] As shown in Figure S2, the leakage current displays a nonohmic characteristic. To reach the critical voltage bias value for ECR, the potential is gradually stepped, as shown in Figure 2a. When the applied voltage is stepped up to 0.8 V (a critical voltage, indicated by the arrow), an increase of baseline current immediately occurs. This time-point indicates the nanopore creation, which is associated with the electrochemical dissolution of MoS_2 enhanced by the ion flow focused on the active site as shown (Figure S3).

In contrast to the avalanche-like dielectric breakdown process in silicon nitride, where a typical 10 min waiting time for the filling of charge traps[9] under the application of critical voltage (>10 V) is needed before breakdown occurs, electrochemical dissolution happens spontaneously at the critical voltage.

In addition, the observed rise of ionic current shows a quite slow rate (~0.4 nA/s). The control on the nanopore size is obtained by using an automatic feedback to cut off the voltage once the desired current/conductance threshold is reached.

DOI: 10.1021/acs.nanolett.5b00768
Nano Lett. XXXX, XXX, XXX−XXX

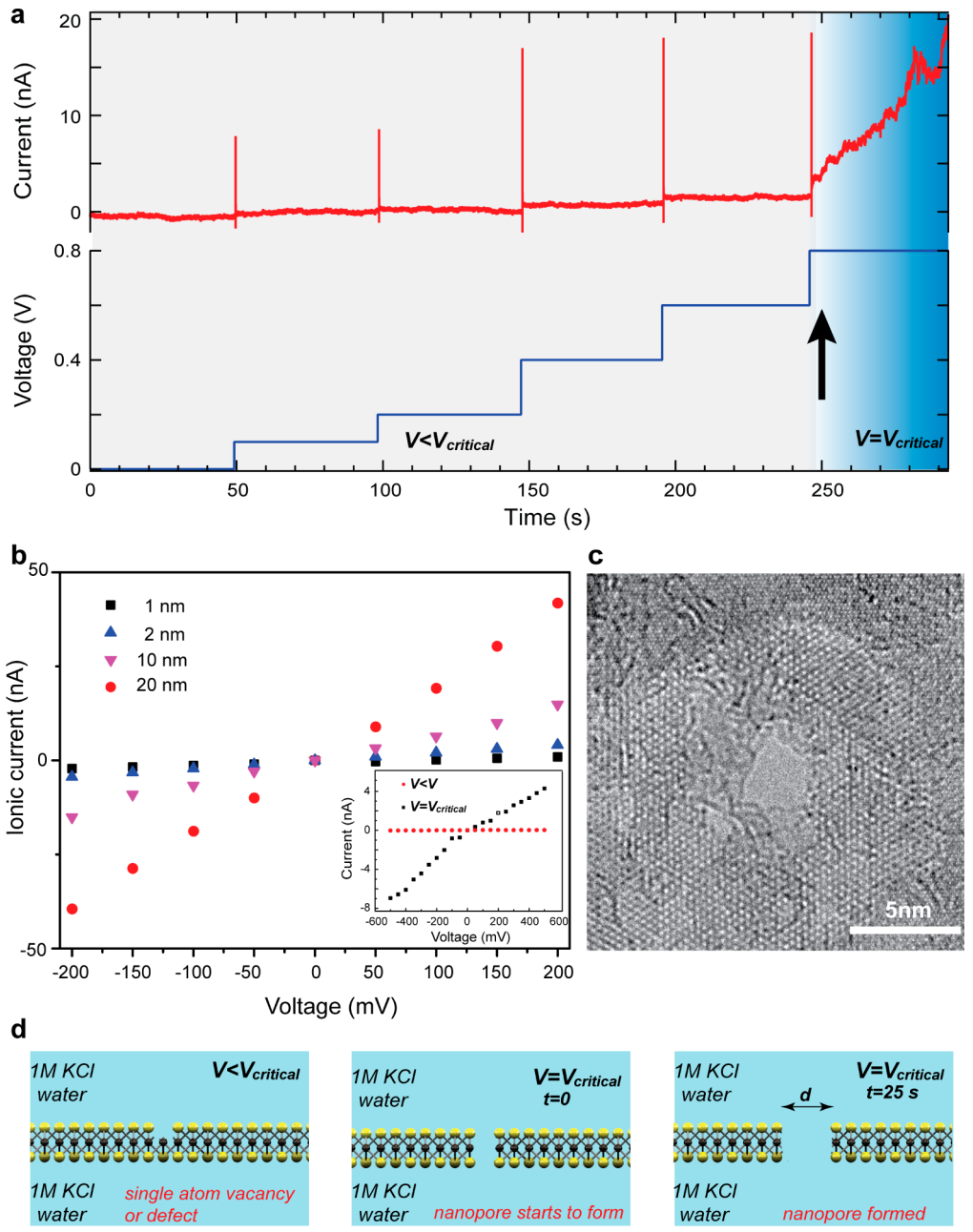

Figure 2. (a) Representative ionic current trace measured for an MoS_2 membrane. Voltage is stepped in 100 mV increments with a 50 s hold time, and the leakage current increases in accordance, being steady for a constant voltage. Sharp peaks at each voltage step originate from the capacitance charging. After a critical voltage of 800 mV is applied,, the electrochemical reaction (ECR) starts (indicated by the black arrow), the current keeps increasing, which triggers the feedback control to switch off voltage bias in order to halt the pore growth (b) Current−voltage (I−V) characteristic of nanopores ranging in diameter from 1 to 20 nm; all nanopores are created via electrochemical reaction. Inset shows I−V characteristics for the system below and at the critical voltage. (c) Cs-corrected TEM image taken at 80 keV incident beam energy verifies the nanopore formation and estimated size (3.0 nm) of nanopore created using ECR. (Diameter measured in image is ∼3 nm.) Corresponding current−voltage (IV) characteristic taken after ECR process and prior to Cs-corrected TEM imaging shown in Figure S4a. Larger area (60 nm × 60 nm) around ECR created nanopore is shown in Figure S4b. (d) Mechanism of ECR based MoS_2 nanopore fabrication. A side view of the monolayer MoS_2 lattice, emphasizing the lattice having single atom (S) vacancy before ECR $V < V_{critical}$, MoS_2 lattice at $V = V_{critical}$, and MoS_2 lattice when nanopore is formed.

This feedback also helps to avoid multiple pore formation. Owing to the limited rates of electrochemical reaction, the MoS_2 nanopore sculpting process is quite slow, occurring on time scales of dozens of seconds to several minutes. Figure 2a gives an example of ionic current trace to reach the threshold of 20 nA, for the critical voltage of 0.8 V.

Taking the advantage of existing theoretical insights to model the conductance-pore size relation,[22] the conductance of the nanopore (G) can be described by[22]

$$G = \sigma\left[\frac{4L}{\pi d^2} + \frac{1}{d}\right]^{-1} \quad (1)$$

DOI: 10.1021/acs.nanolett.5b00768
Nano Lett. XXXX, XXX, XXX−XXX

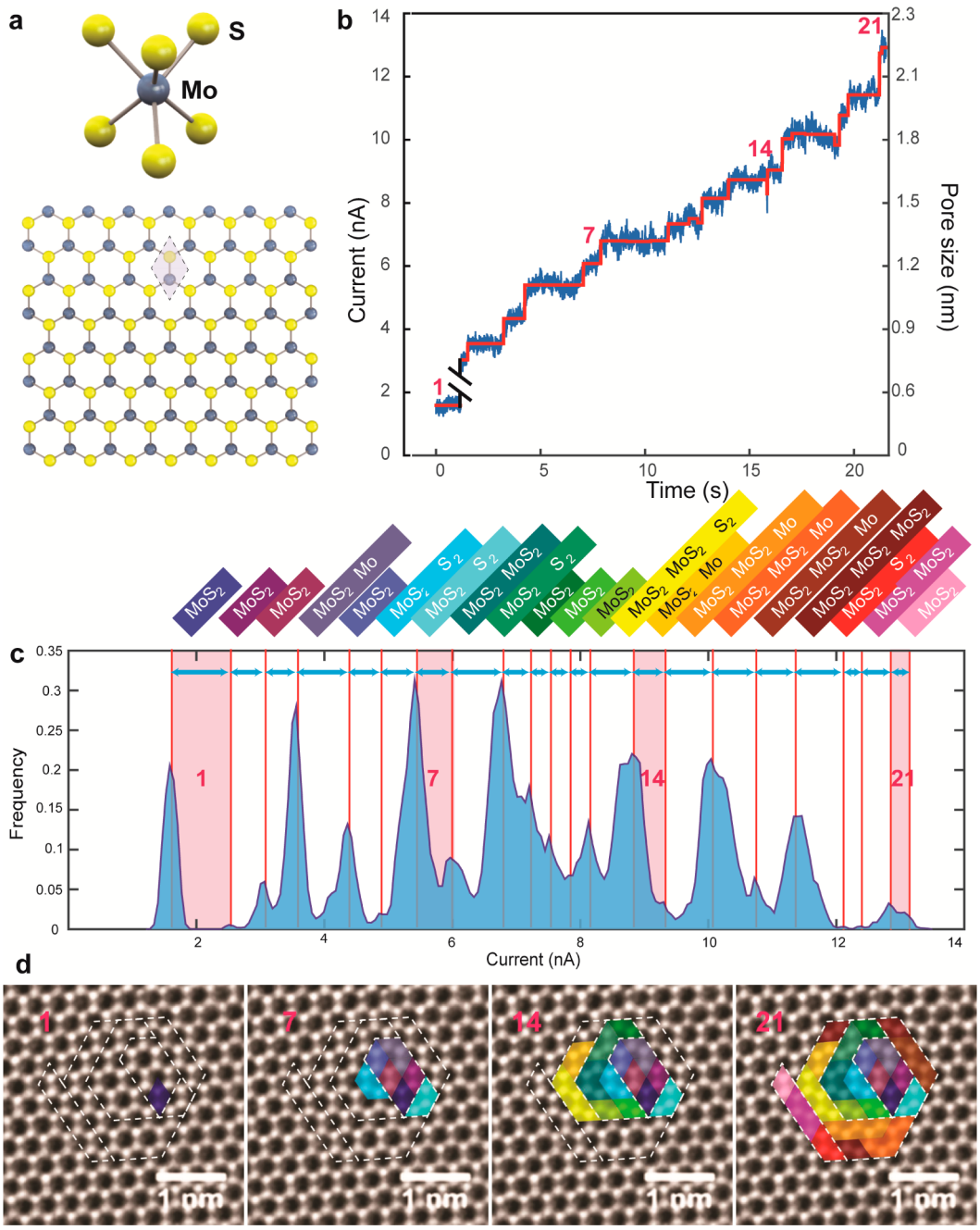

Figure 3. (a) Top view of the monolayer MoS_2 lattice, the unit cell (parameter a = 3.12 Å) is shown in gray.[35] (b) Ionic current step-like features during the nanopore formation in Figure 2a. A custom Matlab code is used to detect steps in the raw trace.[36] (c) Trace histogram shown in panel b with corresponding color coded atom groups cleaved in each step during the pore formation. (d) Illustrative schematic that presents possible outline for nanopore creation. Polygon removal corresponds to the current histogram trace. Cs-STEM micrograph of suspended single layer MoS_2 with superimposed polygons corresponding to atomic groups cleaved in the steps 1, 7, 14, and 21 during the pore formation. The coloring of atom groups cleaved in each step (panel c) and corresponding area polygons shown in the panel d start from violet, blue, cyan, and green to yellow, orange, brown, red, and magenta, analogous to the visible spectrum sequence.

where σ, L, and d are the ionic conductivity of solution, membrane thickness, and nanopore diameter, respectively. Using this relation in combination with feedback on ECR that immediately stops the voltage once the desired pore conductance (corresponding to a certain pore size) is reached, we were able to fabricate pores ranging in diameter from 1 to 20 nm. Figure 2b reveals current−voltage (I−V) characteristics of MoS_2 nanopores fabricated by ECR with different estimated sizes ranging from 1 to 20 nm. The symmetric and linear I−V curves also imply the well-defined shape of the fabricated pores. Similarly, as shown in the inset of Figure 2b, I−V characteristics across the membrane have been investigated in situ before and after ECR, confirming the pore formation.

To further verify the size of fabricated MoS_2 nanopores, TEM has been used to image the newly formed nanopore. Exposure of 2D materials to electron radiation can induce large area damage and also open pores, as reported for both graphene[23−25] and MoS_2.[26] To minimize this risk we imaged the pore using aberration-corrected (Cs) high-resolution TEM (Cs-TEM) at a primary beam energy of 80 keV, using a double-

DOI: 10.1021/acs.nanolett.5b00768
Nano Lett. XXXX, XXX, XXX−XXX

corrected FEI Titan Themis 60−300. (We note that, while aberration-corrected scanning TEM (Cs-STEM) gives more directly interpretable atomic structure contrast, its application here was precluded by residual hydrocarbon contamination from the prior ECR process condensing rapidly under the angstrom-sized probe during imaging. A better sample cleaning procedure would be required to realize successfully Cs-STEM imaging of the ECR pore.) We have first optimized the imaging conditions on the supported portion of MoS_2 outside of the FIB opening and then quickly scanned the suspended monolayer region to find and image the ECR-fabricated pore, all the while taking care to irradiate it minimally. Figure 2c shows the resulting image of an ECR-fabricated MoS_2 nanopore; its current voltage characteristics taken after ECR are shown in Figure S4a, together with a Cs-TEM imaging overview of the surrounding region Figure S4b.

The reliability of fabricating MoS_2 nanopores using the ECR technique is 90%. A few graphene membranes have also been tested by this method, and higher voltages (2−3 V) are required to fabricate pores as presented in the Supporting Information, with the typical ionic current trace displayed in Figure S5.

The described ECR-based pore formation method benefits from the unique crystal structure of transition metal dichalcogenide (MX_2) where atoms are situated in three planes and linked by metal−chalcogenide bonds while in the case of graphene, carbon atoms are in the same plane and three bonds need to be removed to release one carbon atom. In addition, to remove carbon atoms, graphene needs to be oxidized to a higher valence state, which presumably requires a higher voltage bias.

Despite different chemical compositions of transition metal dichalcogenides (MX_2), the pore formation mechanism is in general governed by the electrochemical oxidation reaction that occurs at the location of the defect and requires comparable field strengths to those encountered in SPMs.[17,18] In our case, mechanical avulsion is highly unlikely to occur since the force is insufficient, similarly to previous SPM experiments. The critical voltage of 1.2 V for WSe_2 is in good agreement with our observations (0.8 V for MoS_2), especially if we consider the position in energy of the surface band edges. The physics of the electrochemically fabricated nanopores is determined by the focused electrical field and surface chemistries. The electric field concentrates at surface irregularities or defects, which can be considered as surface active sites, and focuses current flow at the site of the pore and thus locally enhances the electrochemical dissolution, as shown in Figure 2d. The surface dissolution chemistries can be understood as a surface bound oxidation scheme with hole capture and electron injection to produce the MoS_2 oxidation state[27] as shown in

$$MoS_2 + 11H_2O \rightarrow MoO_3 + 2SO_4^{2-} + 22H^+ + 18e^- \quad (2)$$

where MoS_2 is oxidized into MoO_3 and detached into the solution. We believe this reaction is highly likely to happen considering the electrical potential (voltage bias) range we work with. Due to the current technical limitations of electron energy loss spectroscopy (EELS) analysis in the nanopore vicinity, we cannot exclude the possibility that MoS_2 is oxidized to other valence states. Once an active site is removed by the process described above and a very small nanopore has been formed, Figure 2d, due to the fact that the nanopore has a much larger resistance than the electrolyte solution, the flux of the ions will converge toward the pore (Figure S3). This focused ionic current through the pore will locally enhance the electrochemical dissolution as previously described by Beale model.[28] In addition, it is possible that the high number of dangling bonds within the nanopore contributes to the more favorable enlargement of a single nanopore rather than nucleation of many pores. Of course in the presence of many defects, correlated to the material quality in the suspended area, it is hard to eliminate the possibility that one has created multiple pores. By applying a bias voltage higher than the critical voltage at the beginning of the fabrication process it might be possible to observe the formation of multiple pores. Given the stochastic nature of the pore creation process, with our configuration of voltage steps, multiple simultaneous nanoscale ECR events are highly unlikely. Furthermore, feedback control on the applied voltage to obtain the desirable conductance ensures the formation of a single nanopore. Finally, the formation of a single nanopore is verified by TEM imaging. By establishing the correspondence of the nanopore conductance and their size, obtained from TEM images, in the future we hope that this step could be omitted.

The power of ECR-based nanopore fabrication technique, apart from the advantage of being a fast and cheap production lies in the possibility of fine-tuning the diameter of nanopores with unprecedented, single-atom precision. The low nanopore enlarging speed is due to low voltages and the electrochemical dissolution nature of the process. Figure 3b is a 25 s long, continuous pore conductance trace that shows atomic precision during the nanopore sculpting process. The trace starts from the critical point indicated in Figure 2a. Fitting to the conductance-nanopore size relation, we can estimate a pore diameter growth rate of about 1 Å per second. After 25 s, a pore with a diameter of 1.9 nm (area of 2.9 nm^2) has been formed. The area of such a pore is equivalent to almost exactly $N = 34$ unit cells of MoS_2 where the area of the unit cell $u = 0.0864$ nm^2 (Figure 3a).

To our surprise, the growth curve is not linear but step-like, as shown in Figure 3b. Necessarily, the effective size of the pore enlarges with the same step-like characteristic. To gain insights into these step-like features, we plotted the histogram of current values from this trace in Figure 3c, where 21 individual peaks can be extracted from the histogram.

The sequence of the pore size enlargement steps may be normalized by the unit cell area u and a sequence of MoS_2 formula units and Mo and S atoms cleaved (corresponding to 21 current steps) to form the pore may be inferred, as presented in Figure 3c (for details see Supporting Information). Several snapshots of the proposed pore formation process, taken at steps 1, 7, 14, and 21, are displayed in Figure 3d. The full sequence of the pore formation is displayed in Supporting Movie 1. The area of polygons corresponding to the cleaved atom groups follows the honeycomb structure of single-layer MoS_2, as presented schematically in Figure 3a and in the cleavage steps superimposed on a Cs-STEM image of MoS_2 lattice, Figure 3d.

Here presented, step-like features are commonly observed when working with low voltages ranging from 0.8 to 2 V. The reproduced step-like features from other devices is shown in Figure S7. The atomic steps observed here reveal the ultimate precision (single atoms) that can be reached in engineering nanostructures.

To test the performance of ECR-fabricated pores, we performed DNA translocation experiments and detected the

DOI: 10.1021/acs.nanolett.5b00768
Nano Lett. XXXX, XXX, XXX−XXX

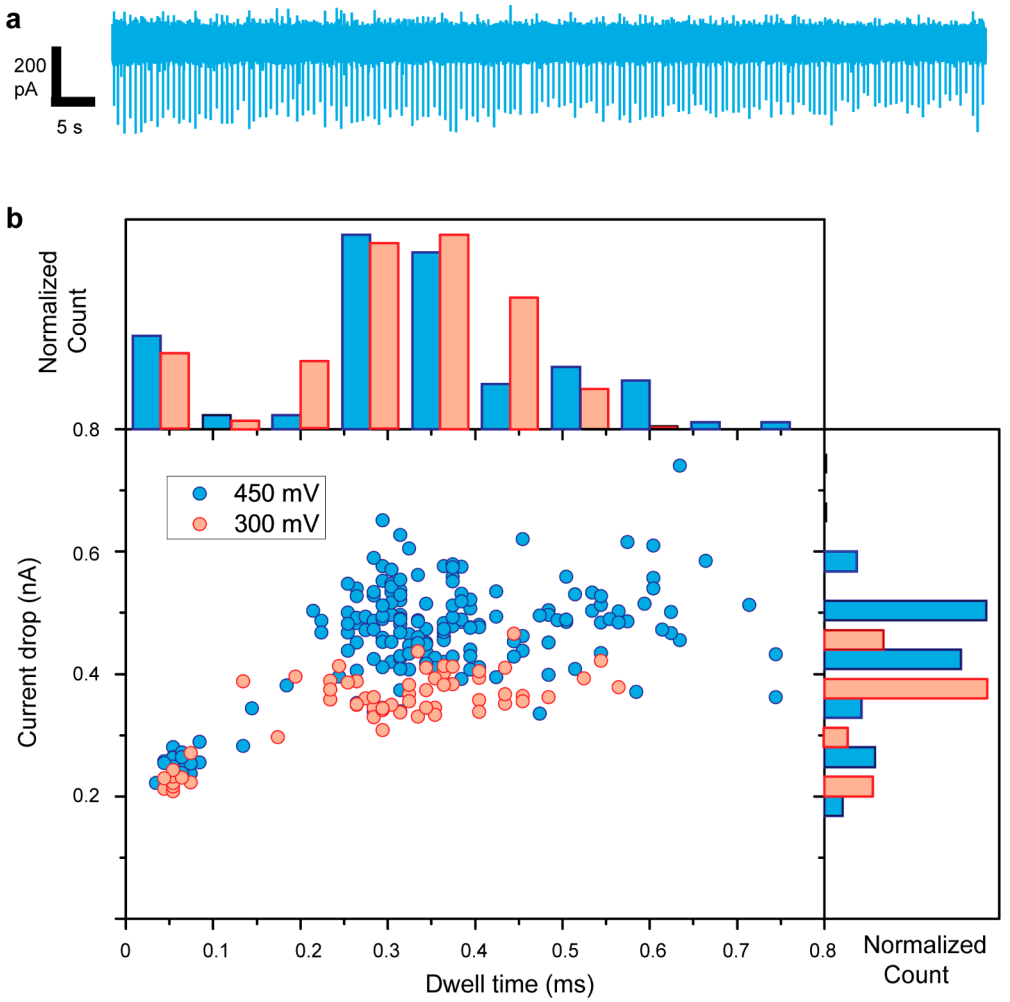

Figure 4. (a) Typical trace of pNEB plasmid DNA translocation through an electrochemically etched nanopore recorded at 450 mV. The trace is downsampled to 10 kHz for display. (b) Scatter plot of events collected at 300 and 450 mV bias. Event detection is performed using OpenNanopore[36] Matlab code. As expected, the increase in the bias shortens the translocation time and enhances the current drop. Considerably longer term operation of the nanopore device is possible since DNA does not adhere to MoS_2, unlike to graphene, as we previously reported.[14,37]

translocation events related to the current drops below the baseline current. ECR fabricated MoS_2 nanopores consistently produce low-1/f noise on the current baseline, which is slightly higher than for TEM drilled MoS_2 nanopores (Figure S8). The major contribution to the 1/f noise in 2D membrane nanopores[29] can be attributed to mechanical fluctuations of the thin membranes. Higher frequency fluctuations are produced by the measurement method itself. Fluctuation noise can be significantly reduced by using a smaller supporting opening[30] or operating at low temperatures. To show the ability of ECR fabricated nanopore for DNA detection, 2.7 kbp pNEB plasmid DNA is translocated through a relatively large MoS_2 nanopore (30−40 nm) to eliminate the pore−DNA interaction and multiple conformation issues. Figure 4a displays only one-level events indicating an extended (unfolded) DNA conformation, with SNR >10. Scatter plots are used to describe the statistics of DNA translocation as shown in Figure 4b. The signal amplitude also increases linearly with the applied voltage, which is 0.5 nA for 450 mV and 0.38 nA for 300 mV as shown in the histogram Figure 4b. Dwell times are also comparable with DNA translocation through a TEM-drilled MoS_2 nanopore of a similar diameter, for the same DNA and under same bias conditions. In addition, λ-DNA (48 kbp) is also translocated through an ECR-fabricated nanopore shown in Figure S9. A noticeable advantage for this nanopore fabrication method is that DNA translocations can be performed in situ after ECR and size-control allows on-demand adaptation of the pore size, allowing sizing for the different types of biomolecules, e.g., proteins[31] or DNA−protein complexes.[32] In addition, to verify the single pore formation for the small nanopore sizes <5 nm, λ-DNA (48 k bp) is also translocated through a 4.3 nm ECR-fabricated nanopore (Figure S9). As shown in Figure S10a, the conductance drop obtained from the simplistic model that assumes two pores would strongly depend on the ratio of the two pore sizes. The experimentally observed blockage of 11% (Figure S9) is in a good agreement with the assumption of a single 4.3 nm pore. For larger pore sizes (15−30 nm), this simplistic analytical model is less reliable since the conductance drop caused by DNA translocation varies slightly (see Supporting Information).

Apart from nanopore sensors, other applications can be further explored based on conductance measurements such as selective ion transport, nanoionics,[33] and atomic switches or as platforms for understanding electrochemical kinetics.[34] To conclude, we present the atomically controlled electrochemical etching of single-layer MoS_2, which we employ to engineer

DOI: 10.1021/acs.nanolett.5b00768
Nano Lett. XXXX, XXX, XXX−XXX

nanopores with subnanometer precision. The fabricated MoS_2 nanopores are carefully characterized by $I-V$ characteristics and their size confirmed by TEM. We attribute the fabrication process to the local concentrated field at surface defects and the electrochemical dissolution of MoS_2. The intrinsic electrochemical reaction kinetics permits the ultimate precision for nanopore fabrication. We have observed step-like features in the ionic current traces, which we attribute to the successive removal of individual atoms. Finally, DNA translocation has been performed to demonstrate the ability of such nanopores in detecting molecules. The ECR nanopore fabrication technique presented here offers a well-controlled method to engineer nanopores at single-atom precision and also paves a practical way to scale up the production of 2D nanopores and commercialize nanopore-based technologies.

■ ASSOCIATED CONTENT

Supporting Information

Experimental methods (setup, CVD MoS_2 growth, transfer of CVD MoS_2 from sapphire to SiNx membrane, graphene CVD growth, finite element analysis model). Detailed data analysis of ionic current steps presented in Figure 3A, reproduced current traces of nanopore formation on MoS_2 membrane using ECR showing discrete steps. The sequence of cleaving MoS_2 unit cells and Mo and S atoms in 21 steps to form the pore (Table S1), power density spectrum (PSD) noise analysis of ECR fabricated MoS_2 nanopore. λ-DNA translocation trace taken at 300 mV. Analytical model that relates conductance drops to the number and size of the pore (Figure S10). Supporting Movie displays the sequence of cleaving MoS_2 unit cells and Mo and S atoms in 21 steps to form the pore. Animation based on Cs-STEM image starts from violet, blue, cyan, and green to yellow, orange, brown, red, and magenta, akin to the visible spectrum sequence. Lifetime of the steps in the sequence is given in the Table S1. These times are used as the cues for the animation; the pore formation process that we have recorded is thus shown in real-time. The Supporting Information is available free of charge on the ACS Publications website at DOI: 10.1021/acs.nanolett.5b00768.

■ AUTHOR INFORMATION

Corresponding Authors

*E-mail: ke.liu@epfl.ch.

*E-mail: aleksandra.radenovic@epfl.ch.

Notes

The authors declare no competing financial interest.

■ ACKNOWLEDGMENTS

This work was financially supported by European Research Council (grant no. 259398, PorABEL. We would like to thank Prof. Xile Hu for useful discussion. M.L. and T.V. acknowledge support by UKF, Grant 17/13, Confined DNA. We thank the Centre Interdisciplinaire de Microscopie Électronique (CIME) at EPFL for access to electron microscopes, and Dr. Sorin Lazar of FEI company for assistance with the Cs-STEM imaging. Devices fabrication was partially carried out at the EPFL Center for Micro/Nanotechnology (CMi) and special thanks to Mr. Joffrey Pernollet for assistance in FIB fabrication.

■ REFERENCES

(1) Novoselov, K. S.; Geim, A. K.; Morozov, S. V.; Jiang, D.; Zhang, Y.; Dubonos, S. V.; Grigorieva, I. V.; Firsov, A. A. *Science* **2004**, *306* (5696), 666−669.

(2) Radisavljevic, B.; Radenovic, A.; Brivio, J.; Giacometti, V.; Kis, A. *Nat. Nanotechnol.* **2011**, *6* (3), 147−150.

(3) Branton, D. *Nat. Biotechnol.* **2008**, *26* (10), 1146−1153.

(4) Dekker, C. *Nat. Nanotechnol.* **2007**, *2* (4), 209−215.

(5) Storm, A. J.; Chen, J. H.; Ling, X. S.; Zandbergen, H. W.; Dekker, C. *Nat. Mater.* **2003**, *2* (8), 537−540.

(6) Park, S. R.; Peng, H.; Ling, X. S. *Small* **2007**, *3* (1), 116−119.

(7) Siwy, Z.; Fulinski, A. *Phys. Rev. Lett.* **2002**, *89* (19), 198103.

(8) Kwok, H.; Briggs, K.; Tabard-Cossa, V. *PLoS One* **2014**, *9* (3), e92880.

(9) Briggs, K.; Charron, M.; Kwok, H.; Le, T.; Chahal, S.; Bustamante, J.; Waugh, M.; Tabard-Cossa, V. *Nanotechnology* **2015**, *26* (8), 084004.

(10) Garaj, S.; Hubbard, W.; Reina, A.; Kong, J.; Branton, D.; Golovchenko, J. A. *Nature* **2010**, *467* (7312), 190−193.

(11) Merchant, C. A.; Healy, K.; Wanunu, M.; Ray, V.; Peterman, N.; Bartel, J.; Fischbein, M. D.; Venta, K.; Luo, Z. T.; Johnson, A. T. C.; Drndic, M. *Nano Lett.* **2010**, *10* (8), 2915−2921.

(12) Schneider, G. F.; Kowalczyk, S. W.; Calado, V. E.; Pandraud, G.; Zandbergen, H. W.; Vandersypen, L. M. K.; Dekker, C. *Nano Lett.* **2010**, *10* (8), 3163−3167.

(13) Liu, S.; Lu, B.; Zhao, Q.; Li, J.; Gao, T.; Chen, Y.; Zhang, Y.; Liu, Z.; Fan, Z.; Yang, F.; You, L.; Yu, D. *Adv. Mater.* **2013**, *25* (33), 4549−4554.

(14) Liu, K.; Feng, J.; Kis, A.; Radenovic, A. *ACS Nano* **2014**, *8* (3), 2504−2511.

(15) Feng, J.; Liu, K.; Bulushev, R.; Khlybov, S.; Dumitru, D.; Kis, A.; Radenovic, A. Identification of Single-Nucleotides in MoS_2 Nanopores. Submitted for publication, 2015.

(16) Karunadasa, H. I.; Montalvo, E.; Sun, Y. J.; Majda, M.; Long, J. R.; Chang, C. J. *Science* **2012**, *335* (6069), 698−702.

(17) Huang, J. L.; Sung, Y. E.; Lieber, C. M. *Appl. Phys. Lett.* **1992**, *61* (13), 1528−1530.

(18) Bohmisch, M.; Burmeister, F.; Boneberg, J.; Leiderer, P. *Appl. Phys. Lett.* **1996**, *69* (13), 1882−1884.

(19) Ataca, C.; Sahin, H.; Akturk, E.; Ciraci, S. *J. Phys. Chem. C* **2011**, *115* (10), 3934−3941.

(20) Dumcenco, D.; Ovchinnikov, D.; Marinov, K.; Lazić, P.; Gibertini, M.; Marzari, N.; Sanchez, O. L.; Kung, Y.-C.; Krasnozhon, D.; Chen, M.-W.; Bertolazzi, S.; Gillet, P.; Fontcuberta i Morral, A.; Radenovic, A.; Kis, A. *ACS Nano* **2015**, *9* (4), 4611−4620.

(21) Walker, M. I.; Weatherup, R. S.; Bell, N. A. W.; Hofmann, S.; Keyser, U. F. *Appl. Phys. Lett.* **2015**, *106* (2), 023119.

(22) Kowalczyk, S. W.; Grosberg, A. Y.; Rabin, Y.; Dekker, C. *Nanotechnology* **2011**, *22* (31), 315101.

(23) Fischbein, M. D.; Drndic, M. *Appl. Phys. Lett.* **2008**, *93* (11), 113107.

(24) Puster, M.; Rodriguez-Manzo, J. A.; Balan, A.; Drndic, M. *ACS Nano* **2013**, *7* (12), 11283−11289.

(25) Traversi, F.; Raillon, C.; Benameur, S. M.; Liu, K.; Khlybov, S.; Tosun, M.; Krasnozhon, D.; Kis, A.; Radenovic, A. *Nat. Nanotechnol.* **2013**, *8* (12), 939−945.

(26) Liu, X. F.; Xu, T.; Wu, X.; Zhang, Z. H.; Yu, J.; Qiu, H.; Hong, J. H.; Jin, C. H.; Li, J. X.; Wang, X. R.; Sun, L. T.; Guo, W. L. *Nat. Commun.* **2013**, *4*, 1776.

(27) Bonde, J.; Moses, P. G.; Jaramillo, T. F.; Norskov, J. K.; Chorkendorff, I. *Faraday Discuss.* **2008**, *140*, 219−231.

(28) Beale, M. I. J.; Chew, N. G.; Uren, M. J.; Cullis, A. G.; Benjamin, J. D. *Appl. Phys. Lett.* **1985**, *46* (1), 86−88.

(29) Heerema, S. J.; Schneider, G. F.; Rozemuller, M.; Vicarelli, L.; Zandbergen, H. W.; Dekker, C. *Nanotechnology* **2015**, *26* (7), 074001.

(30) Garaj, S.; Liu, S.; Golovchenko, J. A.; Branton, D. *Proc. Natl. Acad. Sci. U.S.A.* **2013**, *110* (30), 12192−6.

DOI: 10.1021/acs.nanolett.5b00768
Nano Lett. XXXX, XXX, XXX−XXX

(31) Yusko, E. C.; Johnson, J. M.; Majd, S.; Prangkio, P.; Rollings, R. C.; Li, J. L.; Yang, J.; Mayer, M. *Nat. Nanotechnol.* **2011**, *6* (4), 253−260.
(32) Raillon, C.; Cousin, P.; Traversi, F.; Garcia-Cordero, E.; Hernandez, N.; Radenovic, A. *Nano Lett.* **2012**, *12* (3), 1157−1164.
(33) Maier, J. *Nat. Mater.* **2005**, *4* (11), 805−815.
(34) Valov, I.; Sapezanskaia, I.; Nayak, A.; Tsuruoka, T.; Bredow, T.; Hasegawa, T.; Staikov, G.; Aono, M.; Waser, R. *Nat. Mater.* **2012**, *11* (6), 530−535.
(35) Hulliger, F.; Lévy, F. *Structural Chemistry of Layer-Type Phases*. Springer: New York, 1976.
(36) Raillon, C.; Granjon, P.; Graf, M.; Steinbock, L. J.; Radenovic, A. *Nanoscale* **2012**, *4* (16), 4916−4924.
(37) Husale, S.; Sahoo, S.; Radenovic, A.; Traversi, F.; Annibale, P.; Kis, A. *Langmuir* **2010**, *26* (23), 18078−18082.

DOI: 10.1021/acs.nanolett.5b00768
Nano Lett. XXXX, XXX, XXX−XXX